Die Ergebnisse instrumenteller Beobachtungen deuten darauf hin, dass die horizontale Komponente (BH) des Erdmagnetfelds während der vulkanischen Aktivität verstärkt variiert. In einer Reihe von Observatorien sind die durch das anfängliche Explosionsstadium des Vulkanausbruchs (3. Juli 2019) verursachten Schwankungen durch einen ausgeprägten buchtartigen Anstieg des BH mit einer Dauer von ~ 100 min gekennzeichnet. Daten von anderen Observatorien zeigen einen ausgeprägten alternierenden Charakter der induzierten BH -Variationen mit einer Zeitspanne von ~ 25 min, was für alle Observatorien ungefähr gleich ist. Darüber hinaus sind sowohl im Fall eines buchtartigen Anstiegs als auch bei periodischen BH-Variationen die induzierten Variationen durch eine Amplitude in einem ziemlich engen Bereich von ~ 5 – 14 nT gekennzeichnet. Induzierte geomagnetische Schwankungen in allen Observatorien werden fast gleichzeitig aufgezeichnet. Im Allgemeinen nimmt die Variationsamplitude mit der Entfernung tendenziell ab: von 6 – 12 nT in Entfernungen von bis zu 3000 km bis 2.5 nT in einer Entfernung von ~ 8700 km.

Ein ähnlicher Effekt bei geomagnetischen Variationen wird auch in der zweiten explosiven Phase des Vulkanausbruchs am 29. August 2019 beobachtet. Fast unmittelbar nach der ersten Vulkanexplosion (~ 21:30 UT) wurden scharfe Änderungen von BH in Form buchtförmige positive Variation mit einer Dauer aufgezeichnet etwa 15 min. Nach ~ 20 min wird eine zweite, Bay-ähnliche positive Variation von BH mit kleinerer Amplitude beobachtet, die auf die zweite, schwächere Vulkanexplosion zurückzuführen ist, die in diesem Stadium des Ausbruchs beobachtet wurde.

Während des Zeitraums maximaler Intensität des Abflusses des Aschegasgemisches (6. Juli 2019, ab ~ 01:40 UT) magnetische Observatorien in Entfernungen von weniger als 2700 km verzeichneten charakteristische Veränderungen während des BH in Form von periodischen Variationen mit einer Amplitude in einem engen Bereich von ~ 2,6 – 5,9 nT, trotz des signifikanten Unterschieds in den Entfernungen zum Vulkan.

Die erhaltenen Daten zeigen, dass abnormale geomagnetische Schwankungen nicht nur während der Explosionsperiode, sondern auch während der Ankunftszeit des akustischen Signals am Registrierungspunkt beobachtet werden. Abb. zeigt die geomagnetischen Schwankungen während der Ankunftszeit des akustischen Signals, die durch die Exposition am 3. Juli 2019 in verschiedenen Observatorien verursacht wurden (die aus magnetischen Aufzeichnungen unter Berücksichtigung der Entfernung zur Quelle geschätzte Signalausbreitungsgeschwindigkeit beträgt ~ 295 – 305 m/s).

Literatur

1. Firstov P.P., Akbashev R.R., Zharinov N.A., Maksimov A.P., Manevich T.M., Melnikov D.V. Electrification of eruptive clouds of the Sheluluch volcano depending on the nature of the explosion // Volcanology and seismology. – Russia, 2019. – No 3. – P. 49 - 62.
2. Rossignol J.-C. Magnetic field anomalies associated with geodynamic phenomena // Surveys in Geophysics. –Netherland, 1982. – Vol. 4. – P. 35-454.
3. Sasai Y., Uyeshima M., Zlotnicki J., Utada H., Kagiyama T., Hashimoto T., Takahashi Y. Magnetic and electric field observations during the 2000 activity of Miyake-jima volcano // Earth and Planetary Science Letters. – Netherland, 2002. – Vol. 203. – P. 769-777.

NUMERICAL MODELING OF THE FORMATION HYDRAULIC FRACTURE

A.A. Saifullin, A.M. Zinatullina
Scientific advisor - engineer D.V. Konoshonkin
National Research Tomsk Polytechnic University, Tomsk, Russia

The aim of this report is to model the dynamics of the hydraulic fracture growth depending on the bottom hole pressure in the oil well. The initial and boundary problem describing the process of the hydraulic fracture growth based on PKN model (Fig 1) was defined. Finite-difference scheme was designed using integral interpolational method and it was accomplished by force of C++ code.

The first step in the study concerns determination of the initial and boundary problem with the help of stripe where $0 \le x \le x_{max}, 0 \le y \le y_{max}$ (Fig 2). In the lowest part of the figure there is a fracture in the area $0 \le x \le L_f, 0 \le y \le h$.

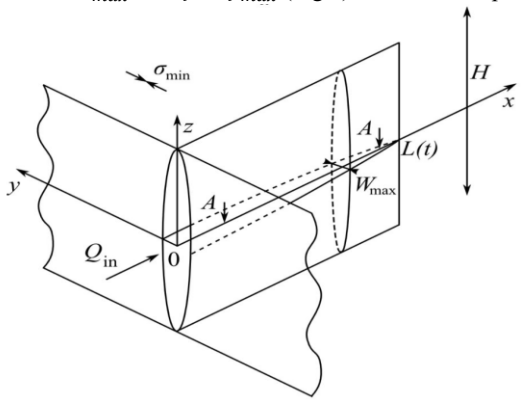

Fig. 1 The hydraulic fracture model

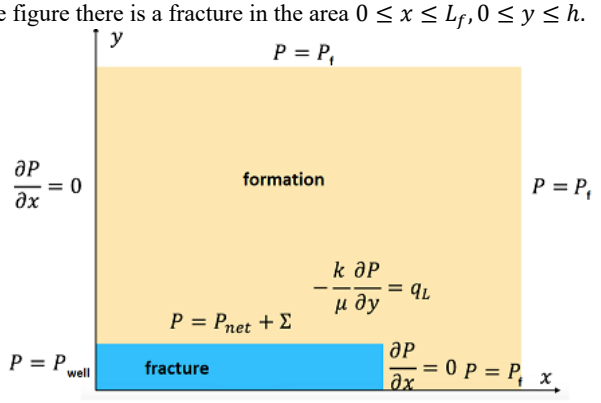

Fig. 2 Boundary conditions

The second step is to design finite-difference scheme:
Modified PKN-model:

$$\frac{\partial P_{net}}{\partial t} = \frac{\partial}{\partial x}\left(\frac{h^2 P_{net}^2}{\mu E'^2}\frac{\partial P_{net}}{\partial x}\right) - \frac{2E'}{\pi h} q_L,$$

Filtration equation:

$$\frac{\partial P}{\partial t} = \chi_0\left(\frac{\partial^2 P}{\partial x^2} + \frac{\partial^2 P}{\partial y^2}\right),$$

Initial conditions	Boundary conditions
$\begin{cases} P_{net}\|_{x\le L_0,t=0} = P_{well} \\ P_{net}\|_{x>L_0,t=0} = 0 \\ P\|_{t=0} = P_f \end{cases}$	$\begin{cases} P\|_{y=y_{max}} = P\|_{x=x_{max}} = P_f \\ P\|_{L_f\le x\le x_{max},y=0} = P_f \\ \left.\frac{\partial P}{\partial x}\right\|_{x=0,h\le y\le y_{max}} = 0 \\ P_{net}\|_{x=0} = P_{well} \\ \left.\frac{\partial P}{\partial x}\right\|_{x=L_f,0\le y\le h} = 0 \\ P\|_{0\le x\le L_f,y=h} = P_{net} + \Sigma \end{cases}$

Then, integral interpolational method was used for solving the problem, specifically central-difference scheme. During the work mass conservation law was used: mass entering the grid block trough the left boundary equals mass leaving the grid block through the right boundary.

After mathematical transformations the following equations were obtained:

$$\begin{cases} \frac{\tilde{P}_{net}\|_i^n - \tilde{P}_{net}\|_i^{n-1}}{\tau} = \frac{A\Delta x}{S}\left[\tilde{P}^3{}_{net}\|_{i+1}^{n-1}\frac{\tilde{P}_{net}\|_{i+1}^n - \tilde{P}_{net}\|_i^n}{\Delta x} - \tilde{P}^3{}_{net}\|_{i-1}^{n-1}\frac{\tilde{P}_{net}\|_i^n - \tilde{P}_{net}\|_{i-1}^n}{\Delta x}\right] \\ \quad + B\frac{\tilde{P}_{i,j}^n - \tilde{P}_{i,j-1}^n}{\Delta y}, \\ \frac{\tilde{P}_{i,j}^n - \tilde{P}_{i,j}^n}{\tau} = \chi_0\frac{1}{S}\left(\Delta y\frac{\tilde{P}_{i+1,j} - 2\tilde{P}_{i,j} + \tilde{P}_{i-1,j}}{\Delta x} + \Delta x\frac{\tilde{P}_{i,j+1} - 2\tilde{P}_{i,j} + \tilde{P}_{i,j-1}}{\Delta y}\right), \\ \tilde{P}_{net}^0\|_{i\le N_0} = P_{well} \\ \tilde{P}_{net}^0\|_{i>N_0} = 0, \\ \tilde{P}_{i,j}^0 = P_f,\ i = \overline{1,N},\ j = \overline{1,M}, \\ \tilde{P}_{net}^n\|_{i=1} = P_{well} \\ \tilde{P}^n\|_{i=N_n} = \tilde{P}^n\|_{i=N_n-1}, \\ \tilde{P}^n\|_{i,j=1} = \tilde{P}_{net}^n\|_i + \Sigma,\ i \le N_n, \\ \tilde{P}^n\|_{i=0,j\ge 1} = \tilde{P}^n\|_{i=1,j\ge 1}, \\ \tilde{P}^n\|_{i>N_n,j=1} = P_f, \\ \tilde{P}\|_{i=N,j} = \tilde{P}\|_{i,j=M} = P_f \quad ,\ i = \overline{1,N},\ j = \overline{1,M} \end{cases}$$

The following results were obtained:

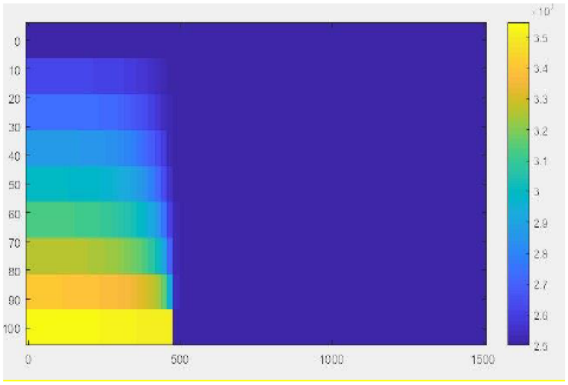

Fig. 3 Pressure distribution in formation

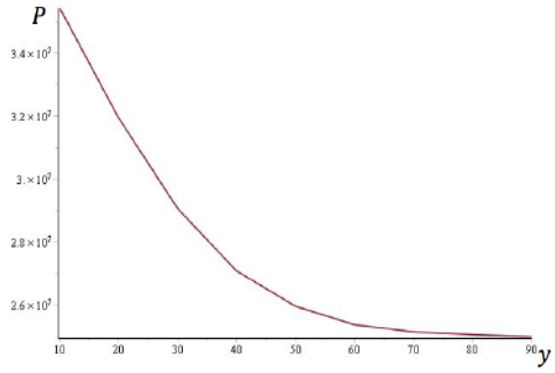

Fig. 4 Pressure dependence on the distance to fracture after 3 hours growth (near the well)

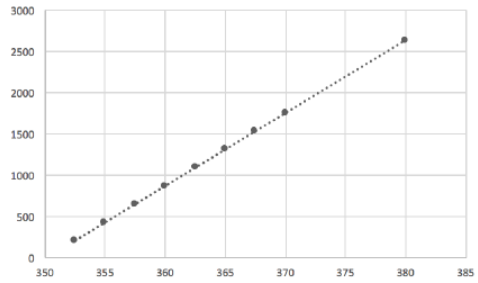

Pressure (atm) bh	Length
352.5	200
355	420
357.2	640
360	860
362.5	1080
365	1300
367.5	1520

Fig. 5 Dependence of fracture length on bottom hole pressure

Calculations for different values of bottom hole pressure were conducted running C++ code and after the dependence of fracture length on bottom hole pressure was found (Fig 6). Obtained time of fracture growth – 24 hours (Table 1). In conclusion, it was determined that during the bottom hole pressure increase the fracture length changes directly proportional. As a result of calculating experiments it was obtained that this dependence is close to linear.

References

1. Nordgren, R.P. Propagation of a Vertical Hydraulic Fracture // Society of Petroleum Engineers Journal. — 1972. — Vol. 12, No 4. — Pp. 306-314.
2. Reservoir Stimulation, 3rd Edition / M.J. Economides, K.G. Nolte. — New York: Wiley, 2000. — 856 p.

MANIFESTATION CENOZOIC VOLCANISM IN EASTERN CHINA AND THE TUNKA RIFT ZONE (BAIKAL RIFT SYSTEM, RUSSIA)

M.I. Saprykina, M.A. Vanteeva, A.A. Semilet, Yu.E. Girenko, Zhang Yongzhan, L.I. Auzina, R.M. Lobatskaya
Scientific advisor - associate professor L.I. Auzina
Irkutsk National Research Technical University, Irkutsk, Russia

Sixty seven million years ago the youngest stage of Earth's development began. At this time, the formation of geological structures characterized by volcanism took place. Volcanoes and volcanic structures are located within both continental and oceanic segments of the Earth.

In an environment of high permeability of the crust, volcanoes erupt, associated with both large zones of extension-continental rifts, and subduction zones.

The Baikal rift system (hereinafter – BRS) is a large arched uplift, the axial part of which is complicated almost throughout by rift depressions. The Baikal rift differs from others in its development in the inner part of the great continent at a considerable distance (2000-2500 km) from the main fronts of the collision of the Pacific plate and the Hindustan subcontinent with Eurasia. The Baikal rift is a unique intraplate phenomenon from the geodynamic and tectonic points of view. [5]

The BRS covers 13 large more or less parallel basins, separated from each other by long high-mountain ridges and low transverse or diagonal bridges, united in 4 rift zones: Muy, Baikal, Tunka, and Khubsugul.

There are two models of Baikal rifting:

1. "active", where the main source of energy is considered to be the flow of magma, the dominant role is played by deep thermal processes that cause melting and thinning of the lithosphere (confirmation-buge anomalies, Dobretsov, 2001.)

2. "passive", in which the main role belongs to the lateral movement of lithospheric plates (in this case – the Eurasian and Indo-Australian).

Most scientists consider these processes as two independent stages of BRS development [2].

The most active manifestation of volcanism occurred in the Tunka rift zone. Tunkinsky rift stretches from the South-Western tip of lake Baikal to the West for 200 km and is an alternation of 5 intermountain depressions filled with Cenozoic deposits with a capacity of more than 2.5 km.

The manifestation of volcanism of the Tunka-Monda group of depressions began in the late Cretaceous-early Paleogene. In the Tunka rift segment, volcanism was activated in several stages: 57-72, 24-36, 8-16, and less than 5 million years ago. Basalts and tuffs of early eruptions were discovered by drilling at the base of the sedimentary-volcanic section of the Tunka depression. Large cracks that caused basalt outpourings were formed in the Miocene-early Pliocene, under conditions of slow deflection of its bottom and uplifting of mountains [4]. In each time interval of the eruption began by olivine tholeiites and ended butanediamine lava packs. At present, there are more than 15 volcanic structures.

Volcanic structures in this zone are very diverse. One of the largest and most well – studied volcanic structures of the Tunka basin is the Khurai-Hobok, composed mainly of tuffs, tufo-breccias, with a high content of manganese, chromium and iron, which caused their color scheme, also noted are volcanic bombs ranging in size from 40 to 270 cm.

Outside the caldera, the rocks are represented by tuff fragments, tuff-breccias ranging in size from 5 to 90 cm.

The occurrence of volcanism in the Eastern part of China was influenced by several factors: the collision of the Indian and Eurasian plates and the subduction of the Pacific plate under the Eurasian plate.